Combustion and Flame 258 (2023) 113062

Contents lists available at ScienceDirect

Combustion and Flame

journal homepage: www.elsevier.com/locate/combustflame

Effect of droplet diameter on oblique detonations with partially pre-vaporized *n*–heptane sprays

Honghui Teng[a,b,c], Cheng Tian[a], Pengfei Yang[d,*], Majie Zhao[a,b,*]

[a] School of Aerospace Engineering, Beijing Institute of Technology, Beijing 100081, PR China
[b] Chongqing Innovation Center, Beijing Institute of Technology, Chongqing 401120, PR China
[c] Advanced Jet Propulsion Innovation Center, Aero Engine Academy of China, Beijing 101300, PR China
[d] State Key Laboratory of High Temperature Gas Dynamics, Institute of Mechanics, Chinese Academy of Sciences, Beijing 100190, PR China

ARTICLE INFO

Article history:
Received 15 February 2023
Revised 31 August 2023
Accepted 6 September 2023
Available online 20 September 2023

Keywords:
Liquid ODWs
Partially pre-vaporized
n–heptane
Eulerian–Lagrangian method
Droplet diameter

ABSTRACT

Liquid fuels have been widely used in propulsion systems for their higher energy density and easier storage, but there are few studies on oblique detonation engines (ODEs) using the liquid fuels. In this study, oblique detonation waves (ODWs) in partially pre-vaporized *n*–heptane sprays are simulated, using a hybrid Eulerian–Lagrangian algorithm with a skeletal chemical mechanism, to facilitate liquid fuels applications in ODE. A novel phenomenon has been observed, illustrating that the ODW initiation lengths in pre-vaporized *n*–heptane sprays firstly increase and then decrease with increasing fuel droplet diameters. It is found out that an increase of droplet diameter can increase the transferred heat amount caused by droplets evaporation and lower the inflow temperature, so leading to the increase of ODW initiation length firstly. However, extremely large droplet diameter can markedly reduce the heat transfer rate of the droplet and its surrounding mixture, and the compressed gas-stream behind oblique shock wave has a higher temperature that accelerate the induction chemical reaction and results in a decrease in the ODW initiation length. Furthermore, the unsteady oscillations of ODW initiation structures are also observed even for a steady inflow, which involves the periodic hot spots, normal detonation waves and their evolutions. Some factors causing the unsteady behavior of ODWs are tested through a sensitivity analysis method of the initiation lengths. Through the analyzation, the fluctuation of the post-shock temperatures is the main factor causing the fluctuation of initiation lengths, revealing that inhomogeneous heat loss by evaporation of dispersed liquid droplets is the main reason causing the unsteady behaviors of ODWs and the competition between heat release by chemical reactions and heat loss by evaporation determines the steadiness of ODWs.

1. Introduction

The oblique detonation wave (ODW) is one kind of extreme combustion which can be induced by a wedge in an incoming, supersonic combustible mixture. Due to compression of the leading shock, ODWs can achieve high thermal efficiency. As a pressure-gain combustion, ODWs have the potential application to ram accelerators [1] and oblique detonation engines (ODEs) [2,3]. In the previous studies, some researchers have done some detonation research with both gaseous fuel and liquid fuel [4–7]. Many basic foundations for ODWs in gaseous mixtures such as the initiation structures [8–10] have been established. Besides, some theoretical analysis of ODWs have also been performed with gaseous mixtures [11–13]. These issues of ODWs in liquid fuels such as kerosene or *n*–heptane mixtures have seldom been reported. However, liquid fuels have the advantages of higher energy density and easier storage and have been widely used in existing propulsion systems [14]. It is necessary to expand the fundamental knowledge of ODWs in liquid fuels as a scientific foundation to facilitate liquid fuels applications in ODE.

For the liquid-gas two-phase ODWs, some works have been performed to study the oblique detonation wave systems. Ren et al. [15] carried out a numerical study of ODWs in two-phase kerosene-air mixtures using the Eulerian–Lagrangian method for the first time to best of our knowledge and the initiation features of two-phase ODWs with different droplet diameters of inflow liquid kerosene are investigated, demonstrating that as increasing droplet diameter, the morphology of ODWs changes from the abrupt wave system to the smooth wave system and the initiation lengths will decrease. Soon afterwards, Ren et al. [16] investigated the effect of the equivalence ratio of the liquid kerosene fuels on ODWs and found that the evaporative cooling effects have more

* Corresponding authors.
E-mail addresses: young1505@foxmail.com (P. Yang), zhaomj@bit.edu.cn (M. Zhao).

https://doi.org/10.1016/j.combustflame.2023.113062
0010-2180/

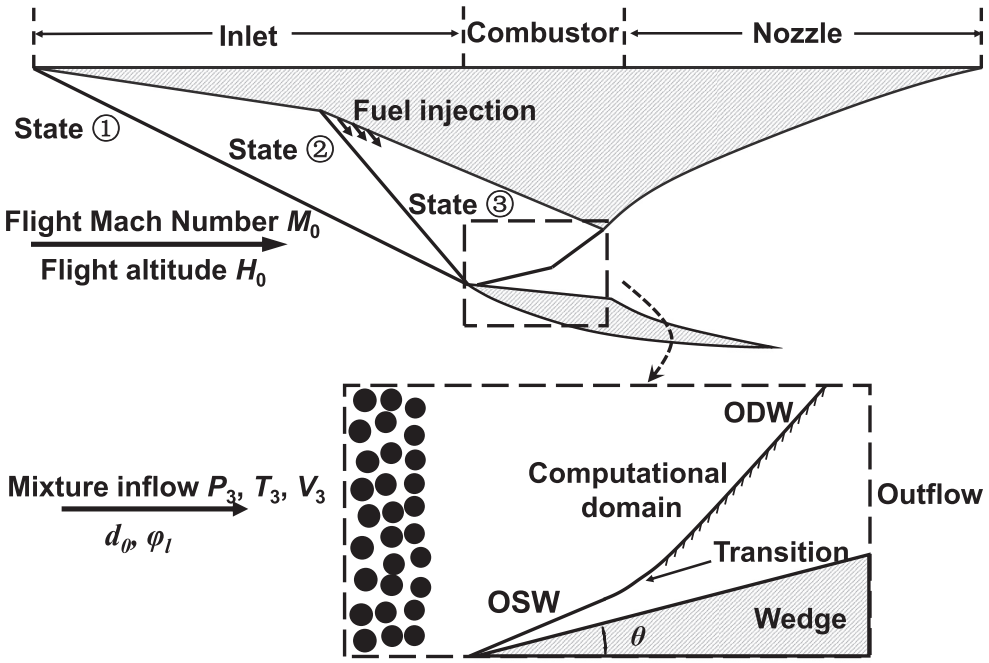

Fig. 1. Schematics of oblique detonation engine and computational zone.

influence in the fuel-lean side, but the heat release effects predominate in the fuel-rich side. However, these above-mentioned investigations used a two-step global chemical reaction model to simulate the detonation combustion and it cannot mimic the accurate heat release processes and reaction rates of all species. Recent researches have demonstrated that the initiation structures are strongly dependent on the chosen reaction models [12]. Besides, the liquid droplets in previous studies [16] is usually assumed to be no pre-vaporized, which does not accord with the practical scenario. Considering the application of ODWs in air-breathing engines in which the airstream is compressed by the inlet and the gas temperature is far larger than ambient temperature, the liquid fuel droplets will be partially evaporated before entering the combustion chamber. Hence, the effects of partially pre-vaporized liquid fuel on ODWs should be considered to facilitate liquid fuels applications in ODE.

Using the hybrid Eulerian–Lagrangian method coupled with a skeletal chemical mechanism, the ODWs in partially pre-vaporized *n*–heptane sprays and air mixtures are first solved. Then the initiation length of ODW and the unsteady behaviors of initiation zone are the important concern of this paper. To analyze the above phenomena, liquid ODWs with different inflow droplet diameters are accurately simulated. Through the numerical results, the liquid ODWs in partially pre-vaporized *n*–heptane sprays have been found and the variations of ODWs initiation structure with droplet diameters are demonstrated. This change of the initiation lengths will be explained by proposing a non-dimensionalized parameter of the amount of transferred heat caused by droplets evaporation and the analyzation of the heat transfer rates along the streamlines. Moreover, what caused this unsteady behavior in liquid ODWs is discussed through a sensitivity analysis method of initiation lengths.

2. Physical models and numerical methods

The schematic of an ODE is used in this work and as shown in Fig. 1, in which the wedge-induced ODW is present. The engine inlet wave configuration is proposed by Dudebout et al. [17] and employed in later researches [18]. Following this configuration, the high-altitude air inflow is assumed to be compressed by two equal-strength oblique shock waves (OSWs) to minimize the entropy increase. Due to the lack of referential engines so far, the injection process is not modeled here. Similar to previous studies [19,20], the inflow fuel-air is assumed to be well-premixed. The supersonic homogeneous inflow reflects on the two-dimensional wedge to generate an OSW and the high post-shock temperature triggers an exothermic chemical reaction and then induces ODW initiation downstream. In this study, the primary focus is on the initiation characteristics of ODWs. Following the previous studies [38,39], is defined as the region located beneath the front of the OSW prior to the onset of the heat release reaction. Accordingly, the initiation point corresponds to the location where the induction reaction on the wedge, and the initiation length refers to the distance between the wedge tip and the initiation point. As shown in Fig. 1, the computational zone used in this study is represented by the region enclosed by the dashed lines. The structured grids are used and the mesh is uniform distribution along the x- and y-direction.

In this study, the hybrid Eulerian–Lagrangian method is employed. The Eulerian gas and Lagrangian liquid droplet governing equations are solved by a compressible two-phase reacting flow solver, *RYrhoCentralFoam* [21,22]. It is developed from *rhoCentralFoam* in OpenFOAM 6.0. For the gas phase, the multi-species Navier–Stokes equations are solved. The liquid phase is modeled as a spray of spherical droplets tracked by Lagrangian method. The inter-droplet interactions are neglected since dilute sprays (volume fraction $<$ 0.001 [23]) are considered. The hybrid Eulerian–Lagrangian method used here has been carefully validated for two-phase detonation [21,24–27], including the numerical study of two-phase ODEs [24], which will not detailed here. To be clear, most of computational models are the same with the previous study [24], including the evaporation model [28], drag force model [29], pressure gradient model, the convective heat transfer rate (the convective heat transfer coefficient is computed using the correlation by Ranz and Marshall [30]), the droplet evaporation heat transfer model and others. Besides, follows the previous study [31] using the same code, the breakup model used in this study is proposed by Pilch and Erdman [32]. Moreover, the liquid fuel of

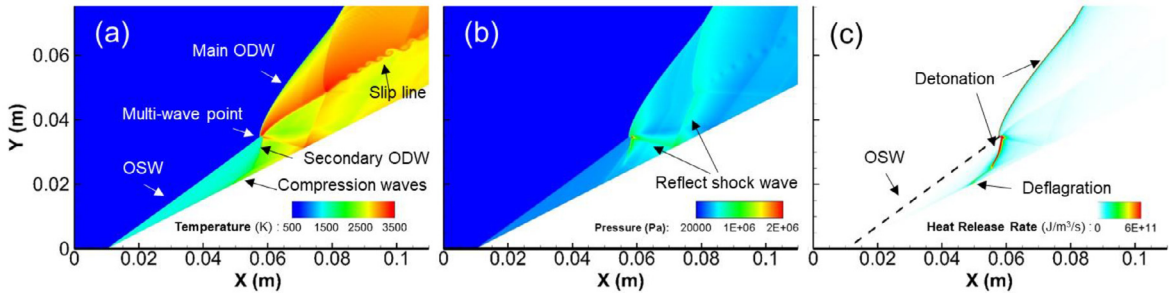

Fig. 2. Temperature (a), pressure (b) and heat release rate (c) fields in the pure gas mixture.

n-heptane is considered and the chemical kinetics model used in this study is a skeletal mechanism of 44 species and 112 reactions [33] for *n*-heptane/air combustion.

For the boundary conditions, inflow condition is used for the left boundary of the computational zone and the zero gradient condition is used for the right and upper boundaries. Some early studies [34] have pointed out that boundary layer effects are negligible under very high Reynolds number. Some recent studies [35,36] have demonstrated that the boundary layer may change the ODW structures, but the effects are weak and limited near the wedge in some cases even with thick boundary layers. For the cases in this study, the thickness of boundary layer near the ignition position is below 5.0% of the induction zone height and the Re number is on the order of 10^6. Hence, following previous ODW studies [37–39], the slip reflecting boundary condition is used and the effect of the boundary layer will be investigated in the future work. On the right of the left boundary, the wedge starts from the $x = 0.01$ m. Because of the multi-scale nature of the phenomena, the computational zone and mesh scale are adjusted respectively. The finest and coarsest mesh of 5 μm and 400 μm are used for different cases in this study and a resolution study on the size scale was conducted, and the results are presented in Appendix A to ensure that a sufficient number of mesh grids were utilized to accurately capture the flow features and phenomena of interest.

To consider the specific flight conditions, the controlling parameters of pre-detonation mixtures are the flight altitude H_0 and Mach number M_0. According to the standard atmosphere [40], the pressure P_0 and temperature T_0 of free inflow are determined by H_0 and the velocity V_0 which is obtained from Mach number M_0 and the local sonic speed a_0. The air inflow is assumed to be compressed by two equal-strength OSWs and based on Rankine–Hugoniot relation with a total deflection angle of 20°, the flow parameters after the compression are calculated and taken as the inflow parameters before the ODW. In this study, H_0 and M_0 are fixed as 30 km and 9.0. Based on the methods introduced above, the pre-detonation parameters are calculated and the inflow temperature T_3, pressure P_3 and velocity V_3 are 697 K, 28,554 Pa and 2535 m/s, respectively. The cases with pure gas and partially pre-vaporized *n*-heptane/air mixture are both simulated and the total equivalence ratio is 1.0 for all the cases. The liquid fuel is modeled as mono-dispersed droplets (which means that all droplets have the same diameter) and the droplets equivalence ratios are 0.3 and the gas equivalence ratios are 0.7 for all two-phase cases. Besides the droplets are under the spherical assumption. The distribution of liquid droplet diameters d_0 is considered to be uniform at left boundary and ranging from 1 to 25 μm. This choice of droplet diameter follows many previous studies [6,7,15] and is similar to the experimental findings of Kindracki [41], where the majority of the droplets had diameters ranging from 20 to 40 μm. The angle of the wedge that supersonic inflow reflects on is fixed as 27°. Moreover, the ambient temperature at 30 km is 227 K and the boiling temperature of droplet at the condition of the inlet duct is about 337 K. Therefore, the droplet temperature is in a range of 227 K to 337 K. In this study, the initial temperature of droplets is fixed as 300 K for all cases, and the effect of droplet temperature is also investigated in *Supplementary Material*.

3. Results and discussion

3.1. ODWs with different droplet diameters

The case in the pure gas mixture of *n*-heptane/air with equivalence ratio of 1.0 is simulated as the base case first, as shown in Fig. 2 by temperature, pressure and heat release rate. First of all, the ODW is initiated in a short distance at such condition and the position of the OSW–ODW transition is around 0.06 m. The OSW–ODW transition is an abrupt type and the OSW and main ODW is connected by a multi-wave point. From the multi-wave point, the reflect shock wave and slip line extend downstream. In the initiation region upstream, the compression waves caused by the heat release of deflagrations arise from the wedge and converge to a secondary ODW. Despite of different chemical reaction mechanisms, this morphology is a typical wave system named 'TYPE III' in ref. [39].

The ODWs in partially pre-vaporized *n*–heptane/air mixture are simulated. The ODW with *n*–heptane sprays of droplet diameter $d_0 = 2$ μm presents an unsteady behavior and as shown in Fig. 3 and temperatures, pressures and heat release rates of six different snapshots of instantaneous flow fields are displayed to illustrate the variation of the wave structure. When $t = 1.715$ ms, as shown in Fig. 3(a1), the OSW–ODW transition is abrupt. Notably, the OSW–ODW transition position is around 0.13 m, longer than that of the case in pure gas mixtures due to the endotherm of droplet evaporation. The OSW and ODW is connected with a multi-wave point. Beneath the multi-wave point, a normal detonation wave (NDW) with large heat release is displayed in Fig. 3(c1). This morphology is similar with the wave system named 'TYPE IV' in ref. [39]. Differently, in front of the NDW, some high temperature hot spots with small heat release appear near the wedge. As shown in Fig. 3(a2-a4), (b2-b4) and (c2-c4), the hot spots trigger the exothermic chemical reaction and a new wave with the intensity of detonation in the induction zone. The new detonation wave moves upward to the OSW and backward to the downstream simultaneously, resulting in a new NDW beneath the OSW and a triple point on the ODW surface as displayed in Fig. 3(a5), (b5) and (c5). Subsequently, as shown in Fig. 3(a6), (b6) and (c6), the new NDW move backward and some new hot spots in front of the new NDW appear again. These new hot spots will transfer into a new NDW in successive times. In generally, this unsteady process with hot spots appearing and the new NDW re-forming repeats in the ODWs with partially pre-vaporized *n*–heptane/air mixture.

The ODW structures and unsteady behavior in case with $d_0 = 5$ μm are displayed in Fig. 4. The main structure of ODW features an abrupt transition, a NDW beneath the transition, reflect

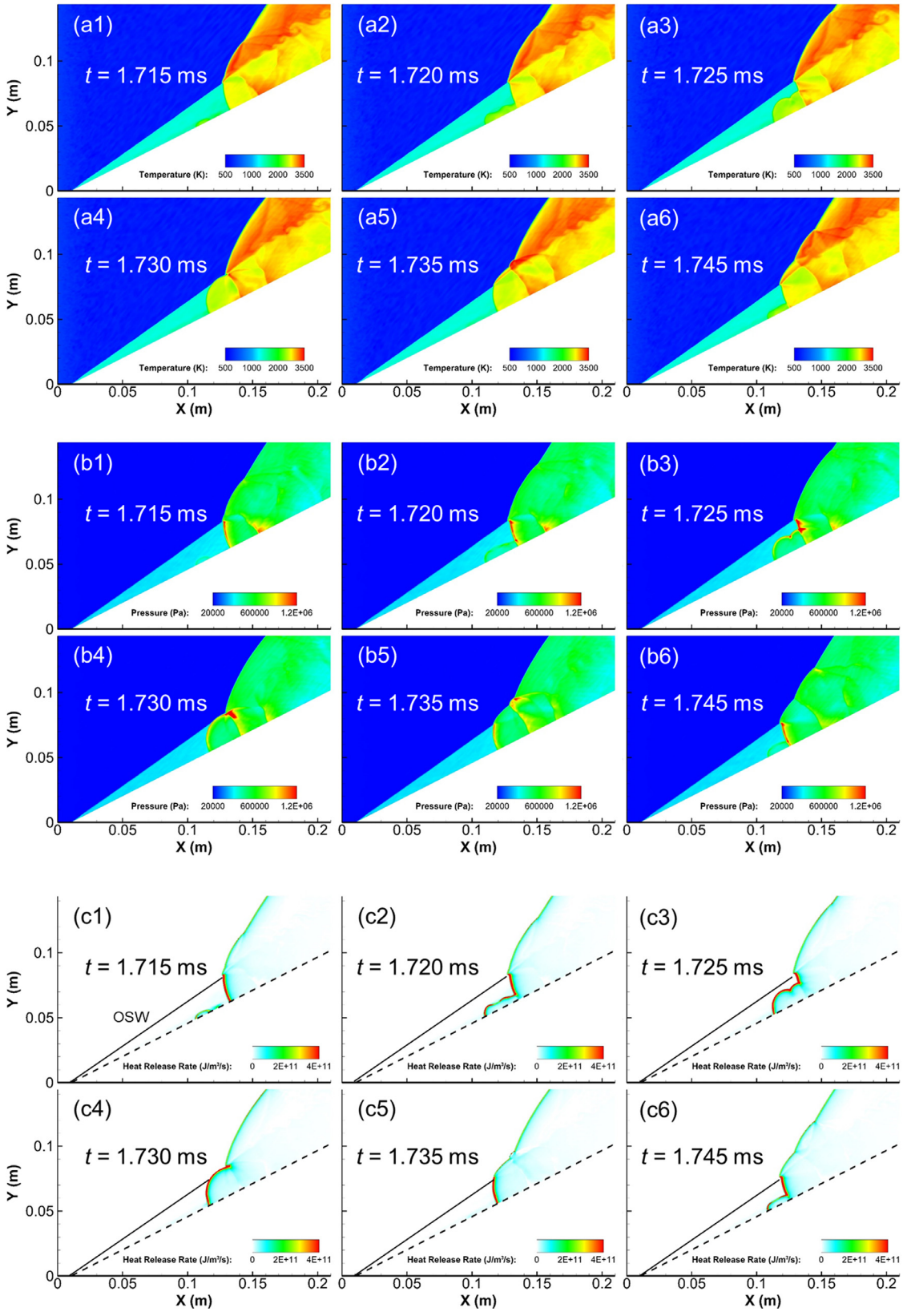

Fig. 3. Temperature (a), pressure (b) and heat release rate (c) fields in partially pre-vaporized n–heptane sprays with $d_0 = 2$ μm.

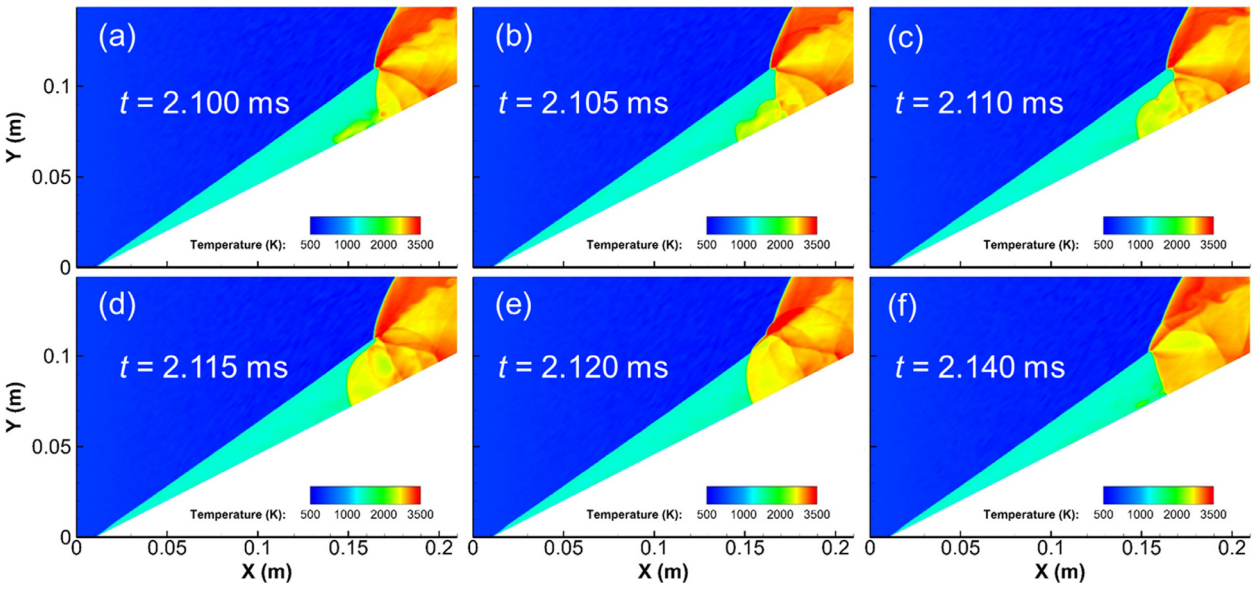

Fig. 4. Temperature fields in partially pre-vaporized n–heptane sprays with $d_0 = 5$ μm.

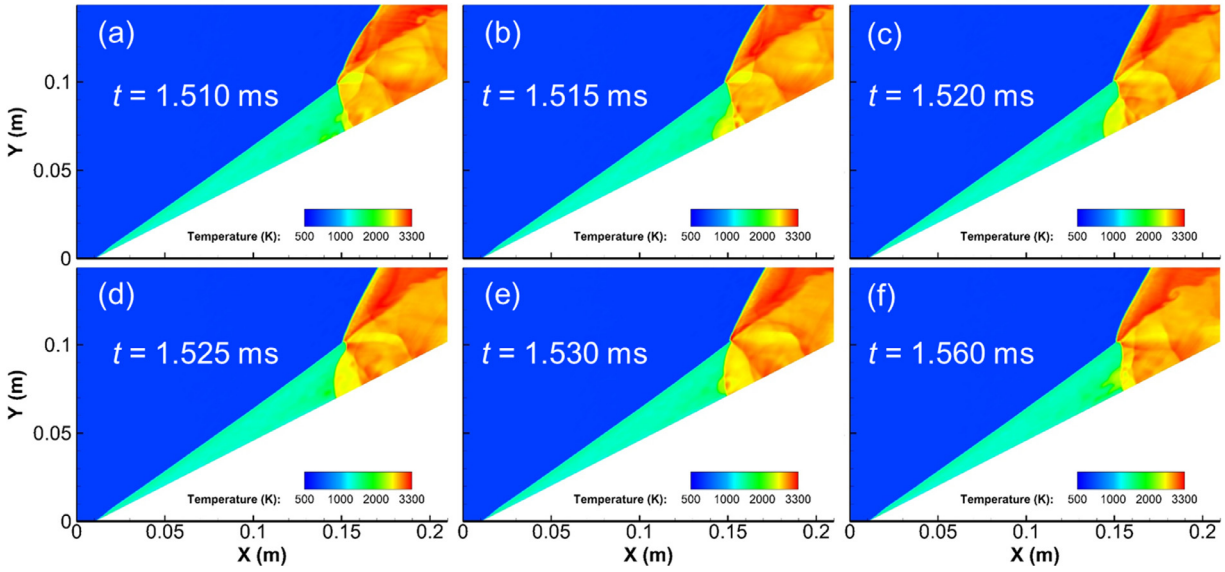

Fig. 5. Temperature fields in partially pre-vaporized n–heptane sprays with $d_0 = 15$ μm.

shock waves and a slip line, similar to that shown in Fig. 3. To further investigate the unsteady behavior, six different snapshots of instantaneous flow fields are presented. As shown in Fig. 3a, when $t = 2.100$ ms, hot spots appear in front of the NDW. The detonation waves are induced by the hot spots then evolve to a new NDW, as shown in Fig. 3(b-e). Subsequently, as shown in Fig. 3f, as the NDW moving backward, the hot spots appear again in front of the new NDW. This unsteady process accompanied by NDW re-forming is similar to the case with $d_0 = 2$ μm. It is worth noting that the OSW–ODW transition position is around 0.16 m, which is longer than that of the case with $d_0 = 2$ μm.

Further increasing the droplet diameter d_0 to 15 μm, the similar ODW structure and unsteady process are observed in Fig. 5. The main structure, i.e., OSW, ODW, multi-wave point, NDW in induction zone, and slip line can be observed in Fig. 5a. As the six different different snapshots of instantaneous flow fields displayed in Fig. 5, the similar unsteady process can be observed, which is hot spot appearing and the new NDW forming and moving backward. However, the OSW–ODW transition position is around 0.15 m, slightly shorter than that of the case with $d_0 = 5$ μm. The scale of the ODW initiation structure decreases when increasing droplet diameter from 5 to 15 μm.

To further investigate the ODWs with big diameter, the case with $d_0 = 25$ μm is simulated. As shown in Fig. 6a, the main structure is present. The OSW–ODW transition is still abrupt and OSW and ODW is connected with a multi-wave point. From the multi-wave point, the NDW, slip line and reflect wave can be observed. Differently, the OSW–ODW transition position is around 0.10 m, which is much shorter than that of the cases with small droplet diameters. The reason of the transition position moving upward will be discussed in next section. To investigate the unsteady behavior of large droplet diameters, six different snapshots of instantaneous flow fields are also presented. Generally speaking, similar unsteady process is observed, including hot spot appearing (see Fig. 6b), new NDW re-forming (see Fig. 6b–e), and moving backward (see Fig. 6f). Notably, a low temperature region can be found near wedge. Similar phenomenon can be found in ref. [24], despite of different chemical reactions. Liquid droplets with big diameter

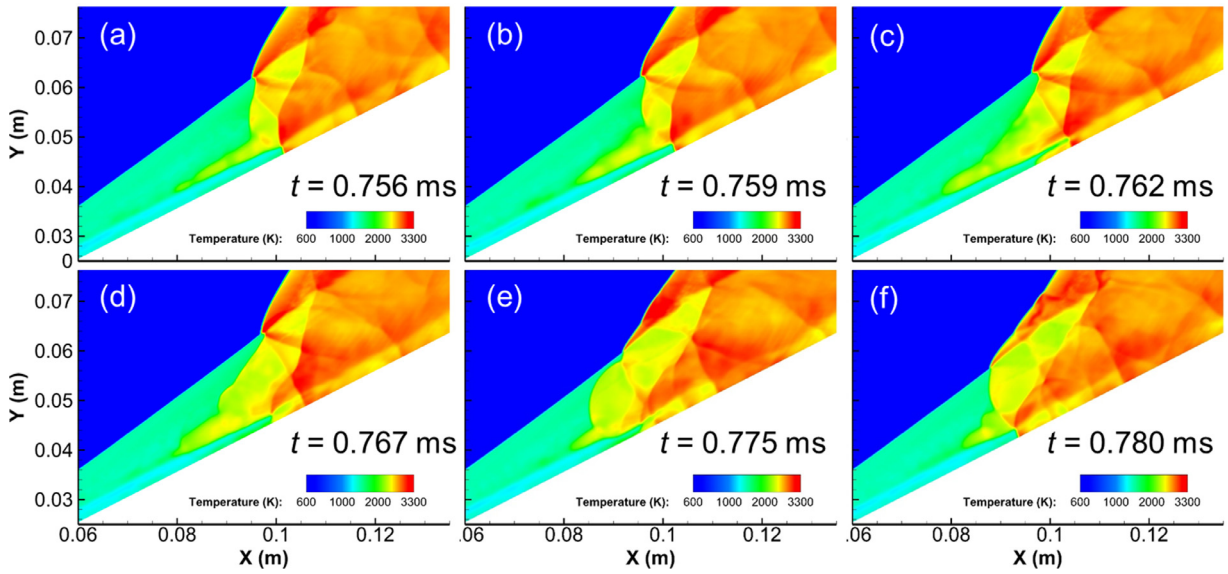

Fig. 6. Temperature fields in partially pre-vaporized *n*–heptane sprays with $d_0 = 25$ μm.

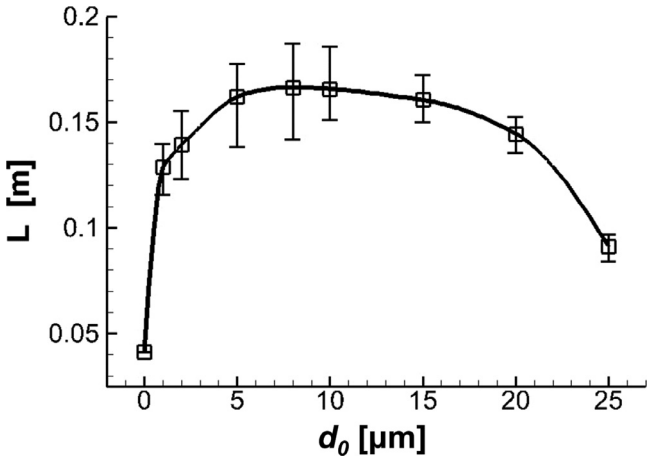

Fig. 7. Initiation lengths as a function of d_0.

or amount are hard to evaporate, leading to the accumulation of droplets near wedge behind the OSW. The low temperature region is caused by the evaporation of droplets near wedge.

As mentioned above, the OSW–ODW transition position changes with the droplet diameter, variation of which is related to the initiation of ODWs. In the previous studies of ODWs in pure gas mixtures [19,38,39], the initiation length is chosen to be an important characteristic parameter to quantify the initiation scale of ODWs. In general, the initiation length is steady in pure gas case, however, in two-phase mixtures the initiation lengths as well as the ODWs' structures are unsteady (see Section 3.1). Figure 7 shows the fluctuating initiation lengths with different droplet diameter. Here, the initiation length is defined as the distance between the front tip and the induction zone where the temperature increases to 110% of the average post-shock temperature along the streamline near wedge. The solid line represents the average initiation lengths over time, and all cases have been simulated for a sufficiently long time to make sure the average initiation lengths tend towards the statistical average. The upper and lower error bars indicate the maximum and minimum values of the initiation lengths for each case. Moreover, the case with $d_0 = 0$ μm represents the ODW in pure gas mixture as shown in Fig. 2. Notably, in the previous study, Ren et al. [15] investigated the effect of the droplet diameters on ODWs using a two-step chemical reaction and only found that the initiation lengths decrease with the increase of droplet diameters without pre-vaporized kerosene sprays. As different fuels and detailed chemical reaction are used in this study, the results are different with partially pre-vaporized *n*–heptane sprays. It can be seen that the average initiation lengths increase rapidly when droplet diameter changes from 0 μm to 1 μm (which means that the inflow fuel changes from the pure gas to gas-liquid mixture). When droplet diameter of the inflow liquid fuel is small ($d_0 < 8$ μm), the average initiation length increases with the initial droplet diameter. However, when further increasing the droplet diameters ($d_0 > 8$ μm), the average initiation length decreases with the initial droplet diameter. Moreover, the fluctuation of the initiation length varies accompanied by the average initiation lengths. The fluctuations of initiation lengths are zero in case with $d_0 = 0$ μm, which is consistent with previous results in pure gas mixtures [37,38]. It can also be found that the fluctuations increase when initiation lengths increase in the cases with small droplet diameters ($d_0 < 8$ μm) and decrease when the initiation lengths decrease in the cases with large droplet diameters ($d_0 > 8$ μm). The reason why initiation lengths changes with droplets diameter will be further explained and the main factor leading to the variation of the initiation lengths fluctuation will be discussed in following parts.

3.2. Initiation lengths for small droplet diameters ($d_0 < 8$ μm)

Figure 8 shows the distribution of droplets evaporation rates for the cases with $d_0 = 2$ μm and 5 μm, respectively. As mentioned above, the initiation lengths increase in the cases with small droplet diameter and this variation of the initiation lengths is related to the droplet evaporation. It can be observed that in cases with $d_0 = 2$ μm, the droplets evaporate completely before the OSW–ODW surface within a certain distance after injected into the ODE. As the d_0 increases to 5 μm, it will take longer for the droplets to evaporate completely and most of the droplets evaporate behind the induction OSW where large evaporation rates are observed.

Since the evaporation of the droplets is accompanied by the heat transfer between the gas mixture and liquid droplets, the increase of the initiation lengths in the cases with small droplet

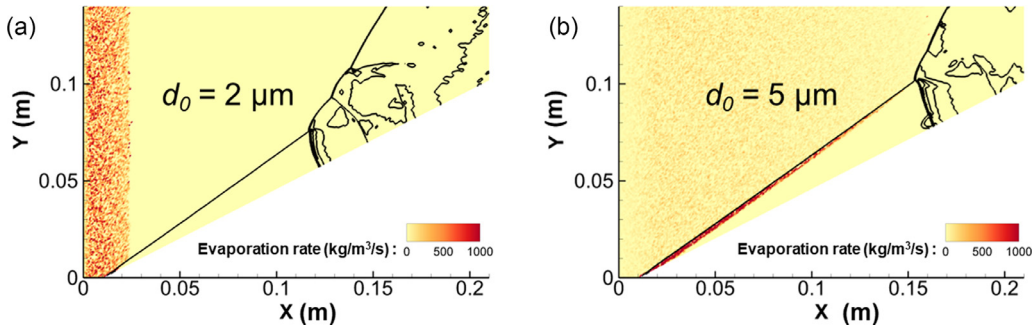

Fig. 8. Distribution of evaporation rates in partially pre-vaporized n–heptane sprays with d_0 = 2 μm (a) and 5 μm (b).

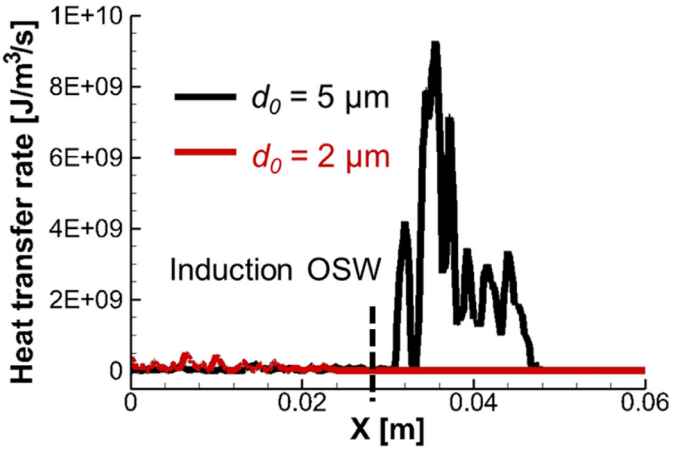

Fig. 9. Droplet heat transfer rates along the streamlines near the wedge in the cases of d_0 = 2 μm and 5 μm. Dashed line represents the location of induction OSW.

diameters may be mainly caused by the droplet evaporation endothermic. To further reveal how initiation lengths are influenced by heat transfer of the droplet evaporation, Figure 9 shows the droplet heat transfer rates along the streamlines near the wedge in the cases with d_0 = 2 μm and 5 μm, respectively. It can be found that the droplet heat transfer position is consistent with the droplet evaporation position shown in Fig. 8. The heat transfer of the droplets occurs before the induction OSW in the case with d_0 = 2 μm, while in the case with d_0 = 5 μm, it mainly occurs after the induction OSW. Moreover, the amount of the local heat transfer rate in the case with d_0 = 2 μm is far less than that in the case with d_0 = 5 μm. This is because the inflow of gas mixtures and liquid droplets decelerates after the OSW, leading to the accumulation of the droplets as well as the compression of the gas mixtures. The increase in the gas temperature and droplet amounts after the OSW causes a large increase in the heat transfer rate of the droplets.

Furthermore, to estimate the influence of the transferred heat of droplet evaporation on the initiation length quantitatively, a heat transfer rate σ dimensionless by the total enthalpy of gas mixtures and an amount of non-dimensionalized transferred heat Q_{eva} are addressed as below:

$$\sigma = \frac{R_d}{h * \rho}, \tag{1}$$

$$Q_{eva} = \int \sigma \, \mathrm{d}t, \tag{2}$$

where, R_d means droplet heat transfer rate whose unit is J/ m^3/s as shown in Fig. 9. h and ρ are the local specific enthalpy and density of gas mixtures, whose unit is J/kg and kg/m^3, respectively. Therefore, σ's unit is 1/s, represents for the local transferred heat rate. Q_{eva} is obtained by the integrating σ over the time it takes for the droplets to travel along the streamline near the wedge, which is non-dimensionalized.

Figure 10(a) shows the distributions of σ along the streamline near wedge in the cases of d_0 = 2 μm and 5 μm. In the case of d_0 = 2 μm, the initiation length is influenced by the heat transfer of droplet evaporation before the induction OSW. For the case with d_0 = 5 μm, the initiation length is not only significantly affected by the heat transfer behind the OSW, but also affected by the heat transfer before OSW. Moreover, it can be also found that the dimensionless heat transfer rate before OSW in the case of d_0 = 2 μm has the same magnitude as that behind OSW in the case of d_0 = 5 μm.

To quantify the total transferred heat, Fig. 10(b) shows the amounts of the dimensionless droplet heat transfer Q_{eva} as a function of droplet diameters d_0 and the average temperature of induction zone. One can see that the Q_{eva} increases rapidly as the average temperature decreases rapidly when d_0 changes from 0 to 1, and the Q_{eva} increases relatively slowly as the average temperature decreases relatively slowly when d_0 further increases. For the cases with small d_0, the results suggest that with increasing droplet diameter, the amount of the transferred heat of droplet evaporation increases, leading to the decease of temperature in the induction zone and the increase of the initiation length.

3.3. Initiation lengths for big droplet diameters (d_0 > 8 μm)

As mentioned in Fig. 7, when the initial liquid droplet diameters increase to large enough (d_0 > 8 μm), the initiation lengths will decrease with the initial droplet diameter. In order to further address the large droplet diameters effects on the ODWs, Fig. 11 shows the distributions of the droplet evaporation rates in the cases with d_0 = 15 μm and 25 μm. It can be found that the large droplets mainly evaporate behind the induction OSW and ODW surface. In the case with d_0 = 25 μm, the droplets evaporate within a longer distance behind the wave surfaces than that in the case with d_0 = 15 μm. To show droplets' evaporation position quantitatively, an equivalent ratio λ among the mole fraction of the carbon, hydrogen and oxygen content in the gas mixtures is proposed as below:

$$\lambda = \frac{X_C/2 + 2X_H}{X_O}. \tag{3}$$

Figure 12(a) shows the distributions of equivalent ratio λ along the streamlines near wedge in the cases with d_0 = 15 μm and 25 μm. Since the initial gas equivalence ratio of the inflow is set to be 0.7, and the equivalence ratio λ keeps constant as 0.7 before the induction OSW in both cases, it indicates that droplets with large diameters hardly evaporate before the OSW and start of the

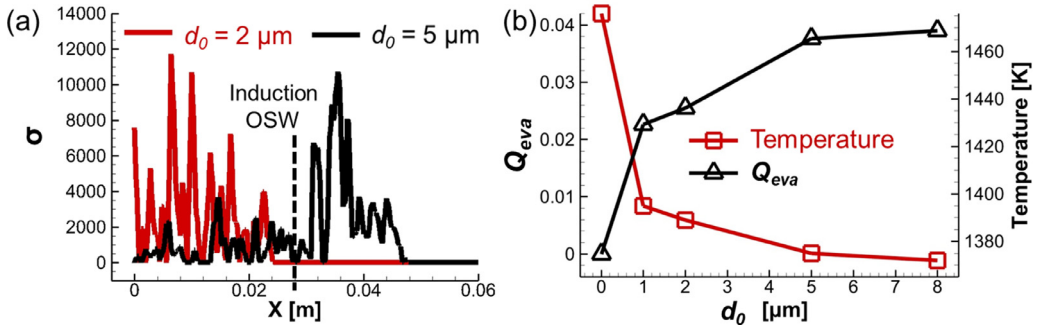

Fig. 10. The dimensionless droplet heat transfer rates along the streamlines near the wedge in the cases of d_0 = 2 μm and 5 μm (a), and the amounts of the dimensionless droplet heat transfer and the average temperatures of the initiations zones as a function of d_0 (b).

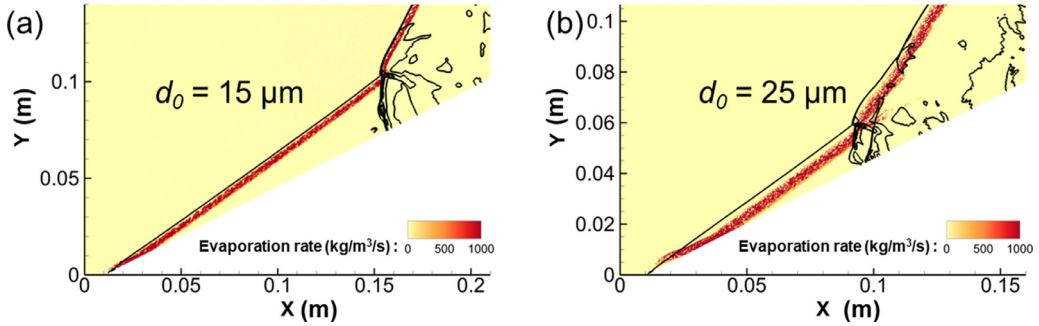

Fig. 11. Distribution of evaporation rates in partially pre-vaporized *n*–heptane sprays with d_0 = 15 μm (a) and 25 μm (b).

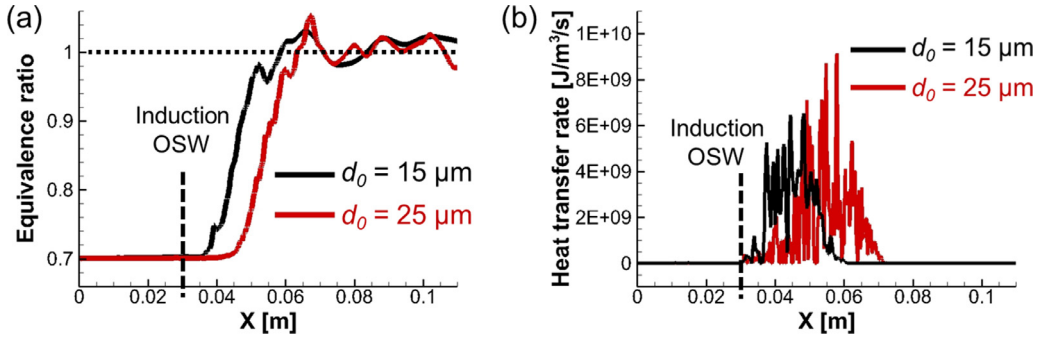

Fig. 12. Equivalence ratios (a) and droplet heat transfer rates (b) along the streamlines near the wedge in the cases of d_0 = 15 μm and 25 μm. The location of the induction OSW is marked by dashed line.

evaporation is behind the OSW. Here, it should be noted that behind the induction OSW, the total equivalence ratio of the inflow including gas and liquid fuels is set to be one, and therefore, the λ will finally increase to 1.0, indicating that the droplets completely evaporate. Moreover, the positions where droplets start and finish evaporating are shifted backward in the case with d_0 = 25 μm due to the slower evaporation with large droplets size. Figure 12(b) shows the distributions of the heat transfer rates along the streamlines near wedge, and it can be found that the droplet heat transfer position in the case with d_0 = 25 μm moves backward as well, which is consistent with the position where the equivalence ratio λ increases sharply (see Fig. 12a).

Figure 13 shows the temperatures and heat release rates along the streamlines near the wedge in the cases of d_0 = 15 μm and 25 μm, respectively. As discussed above, in the case of d_0 = 15 μm, the droplets start evaporation at a shorter distance behind the induction OSW. The cooling effect of droplets with d_0 = 15 μm evaporation causes the temperature behind OSW decrease rapidly as shown in black line in Fig. 13(a). However, in the case of d_0 = 25 μm, for hard evaporation of big inflow droplet diameter the heat transfer rates decrease and the gas mixture behind OSW maintain a higher temperature as shown in red line in Fig. 13(a). As shown in Fig. 13(b), this high temperature leads the higher chemical reaction rates behind OSW and reduces the induction reaction time, which cause the initiation length decrease in the cases of bigger droplet diameters.

3.4. Discussion on unsteady behaviors of initiation structures

The above results suggest that the ODWs in partially pre-vaporized *n*–heptane sprays show significant unsteady behaviors on initiation structures, and the unsteady behavior is related to the fluctuation of initiation lengths. According to refs. [19,38] and [39], the initiation lengths of pure gas case can be obtained by constant volume combustion (CVC) calculation theoretically. Three parameters of post-shock mixture, which are temperature, pressure and equivalence ratio, are used as input of the CVC calculation, leading to the temporal curve of temperature. The theoretical length is deduced by multiplying the induction time (corresponding to 110% of the initial temperature) with the post-shock speed. Therefore, the initiation lengths of ODW can be obtained by four independent parameters, which are pressure, temperature, equivalence ratios and speeds. Figure 14 shows these four parameters of post-shock with fluctuation ranges as a function of droplet diameter. The

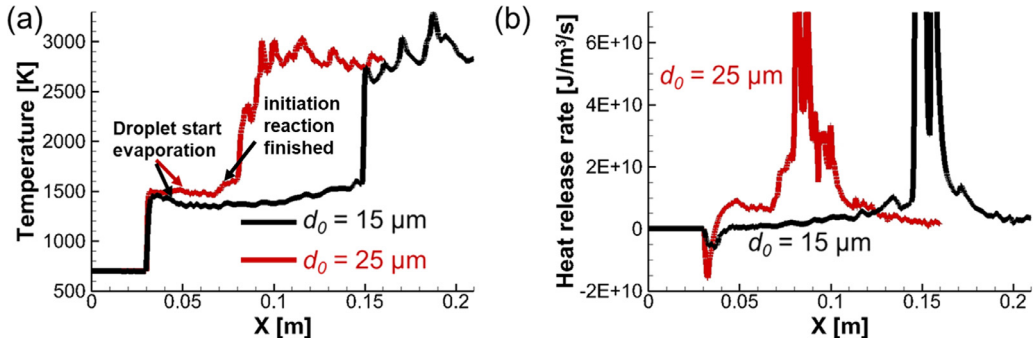

Fig. 13. Temperatures (a) and heat release rates (b) along the streamlines near the wedge in the cases of d_0 = 15 μm and 25 μm.

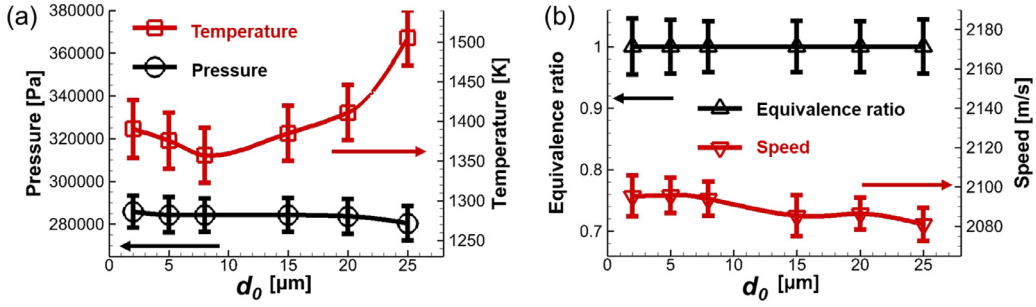

Fig. 14. The pressures, temperatures (a), equivalence ratios and speeds (b) in initiation zone as a function of d_0.

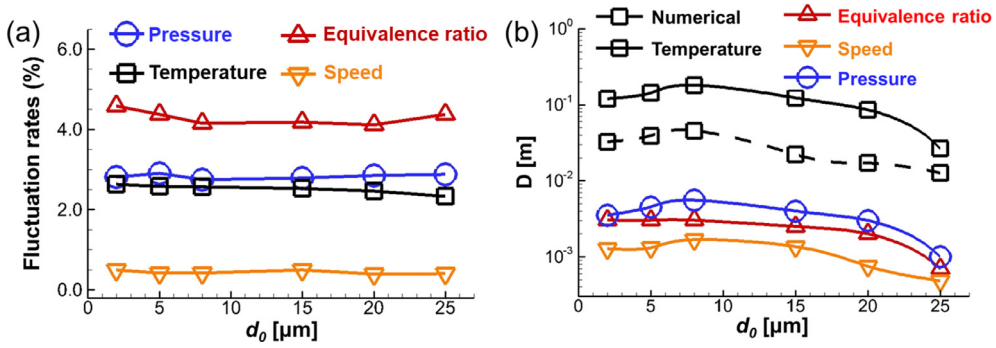

Fig. 15. The fluctuation rates of the pressure, temperature, equivalence ratio and speed in initiation zone (a) and the fluctuation amplitudes of numerical initiation lengths and theoretical initiation lengths caused by different parameters (b) as a function of d_0.

upper and lower error bars in Fig. 14 represent for the maximum and minimum values of each parameter. As discussed above, with the increasing of the droplet diameters, the average post-shock temperature decreases firstly due to the increase of the transferred heat of liquid droplets with small diameters and then increases due to the decrease of the heat transfer rates in the cases with large diameters. Moreover, it is also found that the average equivalence ratio is one since the fuel equivalence ratio of the total inflow gas-liquid mixture is set to be stoichiometric initially. The pressure and speed changes are slightly decreased since the droplet evaporation have a small impact on these two parameters. Generally speaking, besides the temperature, the amount of the post-shock parameters changes slightly as increasing droplet diameter. However, to figure out the main reason cause this unsteady behavior of two-phase ODWs, the deeper analysis is needed.

As talked above, the fluctuation of the initiation lengths may be related to the fluctuation of the four parameters in the initiation zone and in this paragraph, what causes fluctuation of initiation lengths will be discussed. Firstly, to quantity the fluctuation of each parameter, Fig. 15(a) shows the fluctuation rates of the pressure, temperature, equivalence ratio and speed in initiation zone as a function of droplet diameters. Here, the fluctuation rate is deduced by dividing the difference between the maximum and minimum post-shock parameters (as the lengths of error bars shown in Fig. 14) by the corresponding average parameters. It can be seen that the fluctuation rates of all parameters perform a small amount below 5.0% and change slightly with the different droplet diameters. The equivalence ratios have the largest fluctuation rates and the speeds have the smallest ones. Generally, the evaporation of the droplets mainly effects fluctuation of equivalence ratios in initiation zone and has little influence on velocity fluctuation.

To elucidate the relationship between the fluctuation of initiation lengths and the post-shock parameters, a sensitivity analysis method is proposed based on calculation of theoretical lengths. According to the previous studies [38,39], the initiation lengths can be theoretically determined through constant volume combustion (CVC) calculations, showing a good agreement with the numerical ones. This agreement lends support to the assertion that the initiation of ODWs is intimately linked to the induction reaction and underscores the resemblance between the induction process of ODWs and that observed in constant volume combustion. With this method, the fluctuation amplitudes of theoretical initiation lengths caused by the fluctuation of each parameters are estimated by the CVC calculation. Here, the maximum and minimum of one of the four post-shock parameters (for example, the maximum and minimum of temperature) are used as inputs of calculations of the-

oretical initiation lengths separately. By inputting average parameters of other parameters (for example, which are pressures, equivalence ratios and speeds) into these calculations, a small and a large theoretical initiation length can be obtained. The difference between the small theoretical initiation length and the large one will be the fluctuation amplitude of the initiation lengths caused by fluctuation of this parameter (for example, temperature) and the fluctuation amplitudes of temperature in each cases are displayed as solid black line in Fig. 15(b). The fluctuation amplitudes of the theoretical initiation lengths caused by other parameters are obtained with the same way and also displayed in Fig. 15(b). The dashed line in Fig. 15(b) represents for the fluctuation amplitudes of the numerical initiation lengths (as the lengths of error bars shown in Fig. 7) for comparison and the title of *y*-axis represents for difference between the maximum and minimum initiation lengths calculated by each parameter and numerical simulations.

Notably, the average, maximum and minimum of post-shock parameters putted in the theoretical initiation lengths' calculation are extracted through a fixed location on the streamline near wedge behind the induction OSW during this unsteady process. Due to the complex phenomena of ODWs initiation in the cases of different droplet diameters, the selection of this location is depended on the droplet evaporation and induction reaction. In the case with small droplets of 2 μm, due to the droplets evaporation before OSW, this location is the right behind the induction OSW, which is shown in Figs. 9 and 10(a) as marked as 'Induction OSW'. In the case with droplets of 5 and 15 μm, because the droplets completely evaporate behind OSW and before the induction reaction finished, this location is where the droplets finished the evaporation behind OSW as shown in Figs. 10(a) and 12(b), specifically where heat transfer rate turns to zero behind OSW. In the case with droplets of 25 μm, because the droplets evaporate behind the induction reaction finished, to ensure that the initiation is not influenced by heat release, the location is where the induction reaction is finished as shown in Fig. 13(a), specifically where the temperature exhibits a 10% increase compared to the average temperature in the induction zone.

As shown in Fig.15(b) It can be observed that the fluctuation amplitudes of theoretical initiation lengths caused by fluctuation of temperatures are larger than the fluctuation amplitudes of numerical initiation lengths and the fluctuation amplitudes of other parameters are much smaller than the fluctuation amplitudes of numerical initiation lengths. Therefore, the fluctuations of the post-shock temperatures are the main factor causing the fluctuation of the initiation lengths and other parameters have seldom impacts. This means that the inhomogeneous heat loss caused by dispersed liquid droplets in the initiation zone should be responsible for the unsteady behaviors of ODWs. For the fluctuation level of post-shock temperature decrease with the small droplet diameters and increase with large diameters (as shown in Fig 14), the fluctuations amplitudes of numerical initiation lengths perform a corresponding tendency, which increase with small diameters and decrease with big diameters (as shown in Fig 15b). This indicates that the unsteadiness of liquid ODWs is determined by the competition between heat release by chemical reactions and loss by evaporation. In the cases with small diameters, for the amount of transferred heat is increased as raising the droplet diameters, the inhomogeneous heat loss by evaporation plays a more important role and causes a more unsteady behavior of ODWs. In the cases with large diameters, for the reduction of the heat transfer rate behind the induction oblique shock wave, with the acceleration of heat release by chemical reactions of inflow gas mixtures, the ODWs can be initiated in a shorter distance and are steadier. Besides, the results indicate that the dispersed liquid droplets will cause lower fluctuation range of temperatures comparing to that of the equivalence ratio, but this lower fluctuation range of temperatures will cause larger fluctuation range of initiation lengths. This demonstrates that the dispersed droplets will cause a high level of reactant's non-uniformities, but the scale of liquid ODWs initiation is more sensitive to the inhomogeneous heat loss caused by dispersed liquid droplets.

4. Conclusions

In this study, the ODWs in stoichiometric *n*–heptane-air mixtures with equivalence ratio of liquid fuel 30% and different liquid droplet diameters are simulated by using the Eulerian–Lagrangian method with a skeletal chemical mechanism. The results suggest that for the cases with small inflow droplet diameters, the initiation lengths of ODWs increase with initial droplet diameter, which is different from the previous study [15]. Based on the analysis of a non-dimensionalized parameter of the amount of transferred heat, it is found that the reduction of initiation lengths is caused by the increase of transferred heat of droplets evaporation. However, for the cases with large droplet diameters ($d_0 > 8$ μm), the initiation lengths decrease with the initial droplet diameters due to the reduction of the heat transfer rate behind the induction oblique shock wave, and a corresponding high-temperature zone accelerates the induction chemical reaction of the inflow gas mixtures.

Moreover, the initiation structures of ODWs with partially prevaporized *n*–heptane sprays are unsteady, and the unsteady process includes the appearance of the hot spots, re-formation of a new normal detonation wave (NDW) and the NDW moving backward. The scale of ODWs is quantified by the initiation lengths, and it is found that the fluctuation of the initiation lengths is relevant to this unsteady behavior. The main reason that causes this unsteady behavior is analyzed through a sensitivity analysis method. It is found that the fluctuations of the post-shock temperatures are the main reason causing the fluctuations of initiation lengths, while other parameters have little impact, revealing that the inhomogeneous heat loss by evaporations of dispersed liquid droplets in the initiation zone causes the unsteady behaviors of ODWs. Moreover, when the temperatures fluctuate at a low-temperature range, the fluctuation amplitude of initiation lengths will be large and the initiation structure of ODWs will be more unsteady. This indicates that the unsteady behaviors of liquid ODWs are the results of the competition between heat release by chemical reactions and loss by evaporation.

Declaration of Competing Interest

The authors declare that they have no known competing financial interests or personal relationships that could have appeared to influence the work reported in this paper.

Acknowledgments

This research was supported by the National Natural Science Foundation of China (Nos. 12325206, 12202014, 12002041) and Advanced Jet Propulsion Innovation Center, Aero Engine Academy of China (Project ID. HKCX2022-01-018).

Supplementary materials

Supplementary material associated with this article can be found, in the online version, at doi:10.1016/j.combustflame.2023.113062.

Appendix A

As mentioned in this paper, the ODWs in gas-liquid two-phase mixtures have the similar wave structures comparing to the ODWs

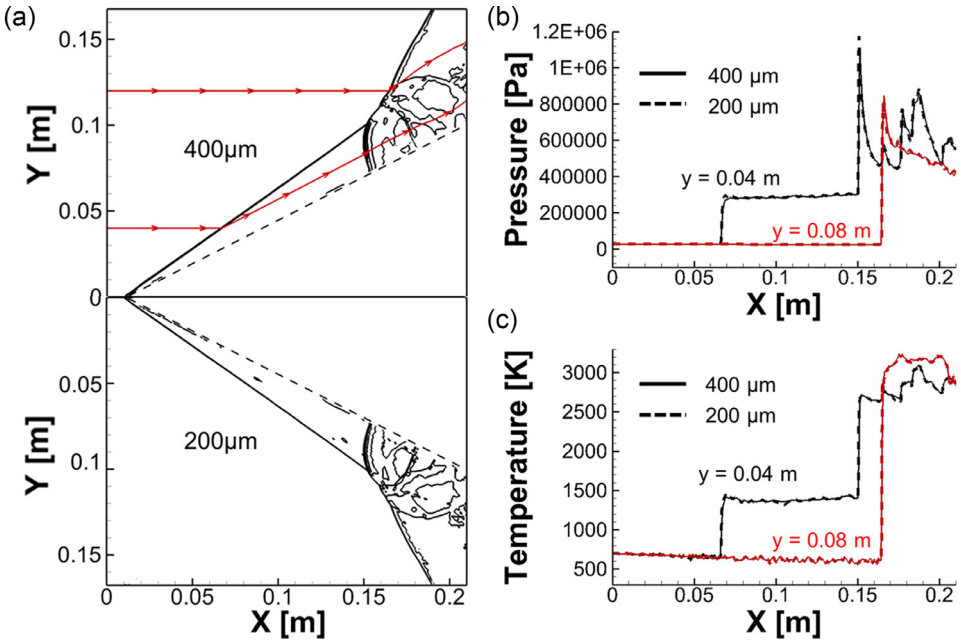

Fig. A. Density fields (a) of ODW in the cases with $d_0 = 5$ μm and different mesh resolutions and the pressure (b) and temperature (c) along the streamlines of $y = 0.04$ m and 0.08 m as shown in figure (a).

in pure gas mixtures and the main problem is whether the grid resolution is sufficient. To examine the effect of grid size, a resolution study is performed by doubling the grid numbers in both x- and y- directions at the same time. For instance, the case with $d_0 = 5$ μm are simulated with a default mesh size of 400 μm and fined mesh size of 200 μm, respectively and the density fields of both cases at $t = 2.100$ ms when the NDW moving backward are displayed in Fig. A(a). The difference between the results of coarse and fine mesh is hard to distinguish. A qualitative comparison of temperature and pressure along the streamlines of $y = 0.04$ m and 0.08 m is conducted, as shown in Fig. A(b). The selected streamline is plotted in the Fig. A(a). These two lines presents two different regions of ODW field, including OSW and main ODW surface. These curves almost overlap, except for slight differences; therefore, the default mesh is sufficient to simulate the ODW. Besides, it can be observed that the pressure will jump to a high level when the streamline passing through the NDW or ODW and then decrease. Due to the complex wave system of ODW downstream, the pressure perturbations can be observed behind. Temperatures experience significant elevation due to the intense compression and energy release induced by the NDW and ODW, resulting in sustained high temperature levels in their wake. For other cases in this study, similar resolution studies have been done to ensure that the sufficient numbers of mesh grids were utilized.

References

[1] A.J. Higgins, Ram accelerators: outstanding issues and new directions, J. Propuls. Power 22 (6) (2006) 1170–1187.
[2] K. Kailasanath, Review of propulsion applications of detonation waves, AIAA J. 38 (9) (2000) 1698–1708.
[3] Z. Jiang, Z. Zhang, Y. Liu, C. Wang, C. Luo, Criteria for hypersonic airbreathing propulsion and its experimental verification, Chin. J Aeronuat. 34 (3) (2021) 94–104.
[4] R. Zhu, X. Fang, C. Xu, Pulsating one-dimensional detonation in ammonia-hydrogen–air mixtures, Int. J. Hydrog. Energy 47 (50) (2022) 21517–21536.
[5] H. Guo, Y. Xu, H. Zheng, Ignition limit and shock-to-detonation transition mode of n-heptane/air mixture in high-speed wedge flows, Proc. Combust. Inst. (2022).
[6] Y. Xu, M. Zhao, H. Zhang, Extinction of incident hydrogen/air detonation in fine water sprays, Phys. Fluids 33 (11) (2021) 116109.
[7] Q. Meng, M. Zhao, Y. Xu, Structure and dynamics of spray detonation in n-heptane droplet/vapor/air mixtures, Combust. Flame 249 (2023) 112603.
[8] Q. Qin, X. Zhang, Study on the effects of geometry on the initiation characteristics of the oblique detonation wave for hydrogen-air mixture, Int. J. Hydrog. Energy 44 (31) (2019) 17004–17014.
[9] Q. Qin, X. Zhang, A novel method for trigger location control of the oblique detonation wave by a modified wedge, Combust. Flame 197 (2018) 65–77.
[10] G. Xiang, Y. Zhang, Q. Tu, The initiation characteristics of oblique detonation waves induced by a curved surface, Aerosp. Sci. Technol 128 (2022) 107743.
[11] D. Martínez-Ruiz, C. Huete, A.L. Sánchez, F.A. Williams, Theory of weakly exothermic oblique detonations, AIAA J. 58 (2) (2020) 236–242.
[12] D. Martínez-Ruiz, L. Scotzniovsky, A.L. Sánchez, F.A. Williams, Wedge-induced oblique detonations with small heat release, AIAA Scitech 2021 Forum, 2021.
[13] Z. Zhang, C. Wen, W. Zhang, Formation of stabilized oblique detonation waves in a combustor, Combust. Flame 223 (2021) 423–436.
[14] G.P. Sutton, O. Biblarz, Rocket Propulsion Elements, 8th ed., John Wiley & Sons, Inc, 2010.
[15] Z. Ren, B. Wang, G. Xiang, Effect of the multiphase composition in a premixed fuel–air stream on wedge-induced oblique detonation stabilization, J. Fluid Mech. 846 (2018) 411–427.
[16] Z. Ren, B. Wang, G. Xiang, Numerical analysis of wedge-induced oblique detonations in two-phase kerosene–air mixtures, Proc. Combust. Inst. 37 (3) (2019) 3627–3635.
[17] R. Dudebout, J. Sislian, R. Oppitz, Numerical simulation of hypersonic shock-induced combustion ramjets, J. Propul. Power 14 (6) (1998) 869–879.
[18] Y.W. Wang, J.P. Sislian, Numerical simulation of gaseous hydrocarbon fuel injection in a hypersonic inlet, J. Propul. Power 26 (5) (2010) 1114–1124.
[19] H. Teng, J. Bian, L. Zhou, Y. Zhang, A numerical investigation of oblique detonation waves in hydrogen-air mixtures at low Mach numbers, Int. J. Hydrog. Energy 46 (18) (2021) 10984–10994.
[20] J. Bian, L. Zhou, H. Teng, Structural and thermal analysis on oblique detonation influenced by different forebody compressions in hydrogen-air mixtures, Fuel 286 (2021) 119458.
[21] Z. Huang, M. Zhao, Y. Xu, G. Li, H. Zhang, Eulerian-Lagrangian modelling of detonative combustion in two-phase gas-droplet mixtures with OpenFOAM: validations and verifications, Fuel 286 (2021) 119402.
[22] M. Zhao, M.J. Cleary, H. Zhang, Combustion mode and wave multiplicity in rotating detonative combustion with separate reactant injection, Combust. Flame 225 (2021) 291–304.
[23] C. Crowe, M. Sommerfeld, Y. Tsuji, Multiphase Flows with Droplets and Particles, Ž, 1998.
[24] H. Guo, Y. Xu, S. Li, H. Zhang, On the evolutions of induction zone structure in wedge-stabilized oblique detonation with water mist flows, Combust. Flame 241 (2022) 112122.
[25] S. Jin, C. Xu, H. Zheng, H. Zhang, Detailed chemistry modeling of rotating detonations with dilute n-heptane sprays and preheated air, Proc. Combust. Inst. 39 (2023) 4761–4769.
[26] Q. Meng, N. Zhao, H. Zhang, On the distributions of fuel droplets and in-situ vapor in rotating detonation combustion with pre-vaporized n-heptane sprays, Phys. Fluids 33 (2021) 043307.
[27] Y. Xu, H. Zhang, Pulsating propagation and extinction of hydrogen detonations in ultrafine water sprays, Combust. Flame 241 (2022) 112086.

[28] B. Abramzon, W.A. Sirignano, Droplet vaporization model for spray combustion calculations, Int. J. Heat Mass Transf. 32 (1989) 1605–1618.
[29] A.B. Liu, D. Mather, R.D. Reitz, Modeling the effects of drop drag and breakup on fuel sprays, SAE Tech. Pap. 102 (1993) 83–95.
[30] W.E. Ranz, W.R. Marshall, Evaporation from drops, Chem. Eng. Prog. 48 (1952) 141–146.
[31] Y. Xu, H. Zhang, Interactions between a propagating detonation wave and water spray cloud in hydrogen/air mixture, Combust. Flame 245 (2022) 112369.
[32] M. Pilch, C.A. Erdman, Use of breakup time data and velocity history data to predict the maximum size of stable fragments for acceleration-induced breakup of a liquid drop, Int. J. Multiph. Flow 13 (1987) 741–757.
[33] S. Liu, J.C. Hewson, J.H. Chen, H. Pitsch, Effects of strain rate on high-pressure nonpremixed n-heptane autoignition in counterflow, Combust. Flame 137 (2004) 320–339.
[34] C. Li, K. Kailasanath, E. Oran, Effects of boundary layers on oblique-detonation structures, 31st Aerosp. Sci. Meet, 1993 Paper No. 450.
[35] C.L. Bachman, G.B. Goodwin, Ignition criteria and the effect of boundary layers on wedge-stabilized oblique detonation waves, Combust. Flame 223 (2021) 271–283.
[36] Y. Fang, Z. Zhang, Z. Hu, Effects of boundary layer on wedge-induced oblique detonation structures in hydrogen-air mixtures, Int. J. Hydrog. Energy. 44 (2019) 23429–23435.
[37] Y. Zhang, Y. Fang, H.D. Ng, H. Teng, Numerical investigation on the initiation of oblique detonation waves in stoichiometric acetylene–oxygen mixtures with high argon dilution, Combust. Flame 204 (2019) 391–396.
[38] H. Teng, H.D. Ng, Z. Jiang, Initiation characteristics of wedge-induced oblique detonation waves in a stoichiometric hydrogen-air mixture, Proc. Combust. Inst. 36 (2017) 2735–2742.
[39] H. Teng, C. Tian, Y. Zhang, L. Zhou, H.D. Ng, Morphology of oblique detonation waves in a stoichiometric hydrogen–air mixture, J. Fluid Mech. 913 (2021).
[40] R.L. King, A Computer Version of the U. S. Standard Atmosphere, 1976, Science Applications, Inc, 1978 Report No.: NASA-CR-150778.
[41] J. Kindracki, Experimental studies of kerosene injection into a model of a detonation chamber, J. Power Technol. 92 (2012) 80–92.